50th AIAA Aerospace Sciences Meeting including the New Horizons Forum and Aerospace Exposition
09 - 12 January 2012, Nashville, Tennessee

AIAA 2012-0870

Computational Optimization of a Natural Laminar Flow Experimental Wing Glove

Fletcher Hartshorn[1]
TYBRIN Corporation, NASA Dryden Flight Research Center, Edwards AFB, CA 93523

Michael J. Belisle[2], Helen L. Reed[3]
Texas A&M University, College Station, Texas, 77843-3141

Under the National Aeronautics and Space Administration's Environmentally Responsible Aviation Program, a laminar flow wing glove is being designed to demonstrate the applicability of swept-wing laminar flow control using discrete roughness elements at chord Reynolds numbers relevant to transport class aircraft. The project, Discrete Roughness Elements Laminar Flow Glove Experiment, will use a Gulfstream III business jet aircraft (Gulfstream Aerospace Corporation, Savannah, Georgia) as a host aircraft for the flight research experiment. The process of developing the wing glove for the project starts with the initial design of a target pressure distribution meeting a set of performance requirements for successful DRE application, assuming an infinite swept wing, and using linear stability theory. An inverse design process produces two initial airfoil shapes that are linearly lofted into a three-dimensional (3D) glove shape, which is mounted and faired on the port wing of a GIII computer-aided design model. The glove shape serves as the initial condition for an optimizer with the objective of producing 3D glove geometry with a spanwise-uniform pressure distribution that matches the target pressure distribution as closely as possible. TRANAIR (Calmer Research Corporation, Cato, New York), a non-linear full potential solver with a coupled boundary layer code is used as the main tool in the design and optimization process of the 3D glove shape. The optimization algorithm uses the Class-Shape-Transformation (CST) method to perturb the geometry with constraints derived from the project requirements and GIII configuration. Results show that with the appropriate inputs, the optimizer is able to match the major features of the target pressure distribution across the entire span of the wing glove. The final glove smoothness and shape were very sensitive to the number of design variables and the format and weighting of the objective function. The number of constraints and design variables also greatly affects the computational time. Linear boundary-layer stability computations demonstrate that stability characteristics conducive to DRE application are nominally achieved across the span of the optimized glove.

I. Nomenclature

A	= design variable array
B	= array of binomial coefficients
C	= class function
C_l	= lift coefficient
C_{local}	= local axial chord length
C_p	= pressure coefficient
C_{pt}	= target pressure coefficient
Dx	= panel length
H	= pressure altitude (ft)
K	= binomial coefficient
M	= Mach number
n	= order of Bernstein polynomial
N	= amplification factor for stability; integral of growth rates
$N1,N2$	= class function exponents
Obj	= objective function

[1] Aerospace Engineer, Aerodynamics and Propulsion Branch, P. O. Box 273; MS 4840B, AIAA Member.
[2] Graduate Student, Department of Aerospace Engineering, TAMU MS 3141, AIAA Member.
[3] Professor, Department of Aerospace Engineering, TAMU MS 3141, AIAA Fellow.

Q_∞ = freestream upstream velocity
Re_c = local chord Reynolds number
S = shape function
U_∞, W_∞ = leading-edge-normal and leading-edge parallel freestream upstream velocities, respectively
X/C = non-dimensionalized axial coordinate
Y/C = non-dimensionalized spanwise coordinate
Δx = x coordinate perturbation
Δz = z coordinate perturbation
Λ = leading-edge sweep angle
f = disturbance frequency (kHz)
λ = spanwise wavelength (mm) parallel to the leading edge
η = Y/C
Ψ = X/C
ζ_i = Bezier curve

Acronyms

2D = two-dimensional
2.5D = describing an infinite-swept wing; that is, derivatives of flow quantities are zero in the direction parallel to the leading edge
3D = three-dimensional
BL = aircraft buttock line (in)
CAD = computer-aided design
CF = crossflow
CFD = computational fluid dynamics
CST = class-shape-transformation
DFRC = Dryden Flight Research Center
DR = design run
DRE = discrete roughness elements
DRELFGE = Discrete Roughness Elements Laminar Flow Glove Experiment
ERA = Environmentally Responsible Aviation
GIII = Gulfstream III
LE = leading edge
LPSE = linear parabolized stability equations
LST = linear stability theory
NACA = National Advisory Committee for Aeronautics
NASA = National Aeronautics and Space Administration
NLF = natural laminar flow
RMS = root mean square
SCRAT = SubsoniC Research AircrafT
TE = trailing edge
TS = Tollmien-Schlichting

II. Introduction

The National Aeronautics and Space Administration (NASA) Dryden Flight Research Center (DFRC) (Edwards, California) performs a significant amount of flight research into new technologies that benefit aviation. One current project at DFRC is the Discrete Roughness Elements Laminar Flow Glove Experiment (DRELFGE), a cooperative effort with the Flight Research Laboratory at Texas A&M University (College Station, Texas). The purpose of DRELFGE is to demonstrate the capability of using discrete roughness elements (DRE) to delay laminar-turbulent transition on a swept wing in flight at Reynolds numbers comparable to transport class aircraft. The capability of DRE as a technology for swept-wing laminar flow control in wind tunnel tests and in flight (at lower Reynolds numbers than DRELFGE) has been established.[1]

The concept selected for this demonstration is an instrumented wing glove[2] which uses a Gulfstream III (GIII) business jet (Gulfstream Aerospace Corporation, Savannah, Georgia) as a test bed. This test bed is named the SubsoniC Research AircrafT (SCRAT) and is operated from NASA DFRC. The glove will be placed on the port wing of the aircraft and is approximately six feet in span. The initial glove shape described previously[3] began with the design of a target pressure distribution meeting a set of performance requirements. An infinite swept wing was assumed and linear stability theory was used to shape the pressure distribution conducive to DRE application. An inverse design process coupled with geometric constraints was then applied to produce two airfoil shapes that were then lofted into a three-dimensional (3D) glove, which

was mounted and faired on the port wing of a computer-aided design (CAD) model of the GIII. When the Navier-Stokes simulation of the full GIII aircraft (including the glove and fuselage and engine effects) was run, the resulting pressure distribution on the glove test article did not have the required characteristics to support a successful DRE flight research experiment. To correct this problem, this 3D initial glove design will be optimized to maintain spanwise uniform flow that produces the required conditions and boundary layer properties to yield a successful experiment.

In the last few decades, computational optimization has played a major factor in the design of aircraft wings. Before optimization, the design of wings consisted of running a parametric study of many different designs, which had to be analyzed and wind tunnel tested. With the advent of computational optimization, where a flow solver is linked with a numerical optimization procedure; aircraft wings, configurations, or any other shape can be designed in short order to meet a specific set of requirements while satisfying real world constraints.[4-6] For example, an aircraft wing can be designed to minimize the drag produced, while maintaining structural integrity, and enough room for fuel in the wings by adding realistic span and thickness constraints. Drawing from the previously developed tools and experience in designing wings, an optimization process can be setup to complete the design of the wing glove for DRELFGE. It needs to be noted, however, that computational fluid dynamics (CFD) has been improved upon tremendously over the last few decades, but there are still a lot of inherent assumptions and models that are not physically real. Therefore, a computational optimization routine using CFD can be very useful for preliminary design and analysis, but should be supported with wind-tunnel or flight testing to cement its validity. It is for this exact reason that computational optimization of the wing glove is perfect for this project. It will be designed using the method prescribed in this paper, and will be flight-tested to determine its quality and validity towards future designs.

III. Geometry and Grid Topology

The wing glove is placed on a GIII, which is a low-wing business jet, with aft body mounted engines, and a T-tail. The GIII aircraft was chosen for this flight research experiment mainly because it has a chord length that is very comparable to transport category airplanes such as a Boeing B737 (The Boeing Company, Chicago, Illinois). Additionally NASA DFRC already has much experience and data on the GIII aircraft, which made it a logical choice as a test-bed for the DRELFGE experiment.

A. Geometry

The glove seen in Fig. 1, is placed on the port wing starting at approximately the 45% half span location.[2]

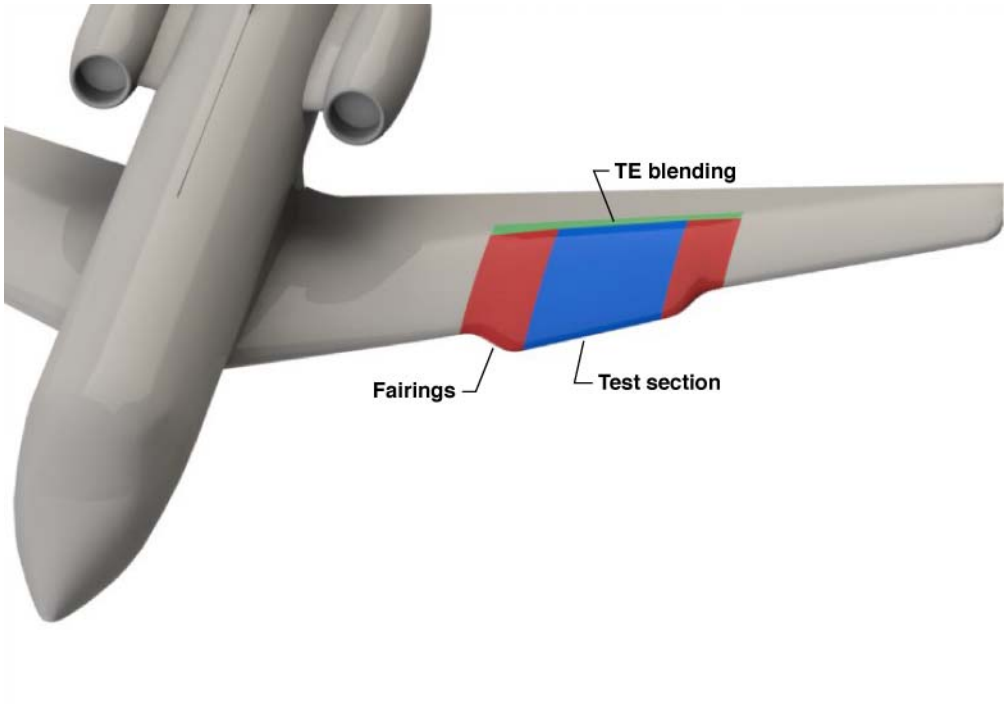

Figure 1. Glove mounted on the left wing (test section shown in blue; fairings shown in red; TE blending shown in green).

The blue piece is the main test section; the red are the fairings with smooth tangency and curvature blending (both inboard and outboard) with the original GIII wing; the green part is the blending region again with smooth tangency and curvature

blending aft of the 60% chord location. The inboard and outboard fairings are 3.2 ft and 2.5 ft in span, respectively. The glove geometry is offset from the wing with two inches of clearance, and protrudes from the leading edge (LE) of the wing by 2.3 ft.

Initial results for the 3D glove optimization are computed using only the wing and the glove to reduce the computational time. The final configuration used for the optimization includes the wing with the mounted glove, the aircraft body, and the engine. The T-tail was not included because it is located far enough away as to not have any influence on the local flow over the wing glove.[7]

B. Grid Topology

The 3D optimization process starts with a full-aircraft TRANAIR (Calmer Research Corporation, Cato, New York) simulation. TRANAIR uses a fully structured grid to discretize the surface geometry with a combination of point matching and linear abutments.[8] The surface grid is created for the wing only geometry, as well as the wing/body/engine configuration seen in Fig. 2. The wing-only grid is created with the same parameters as the wing grid for the wing/body/engine configuration. Even though the glove is placed only on the port wing on the actual flight experiment aircraft, a symmetry plane was used for both configurations to reduce computational time. Since a symmetry plane is used, the aircraft grid is mirrored to the right hand side in order to better integrate with the TRANAIR solver.

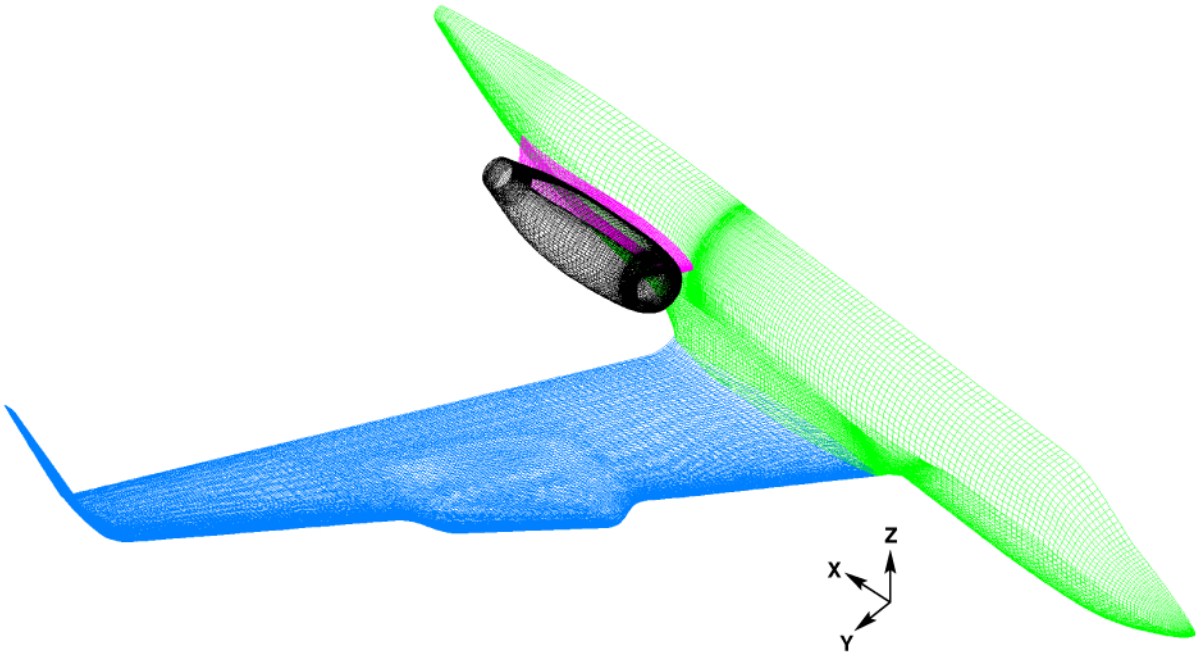

Figure 2. Fully structured surface grid (wing/glove shown in blue; body shown in green; pylon shown in magenta; engine shown in black).

The volume grid for each solution is automatically generated by TRANAIR and adapted to refine flow features. The final volume grid is obtained by a sequence of successively refined grids that are adapted based on errors in the velocity gradients, and user inputs.[8] This allows the Cartesian grid to adapt to non-linear flow-features such as suction peaks and oblique shocks.

IV. Design Process Methodology

The glove is being designed in three main stages: 1) creating a target infinite-swept-wing C_P design conducive to DRE control and termed 2.5D, 2) generating an initial 3D glove shape, and 3) optimizing the full 3D glove design meeting the target C_p distribution. The entire design process is outlined using a flow chart in Fig. 3, where Blocks 1, 2, and 3 outline the target infinite-swept-wing C_p design, initial glove-shape design, and full 3D glove design and optimization process, respectively.

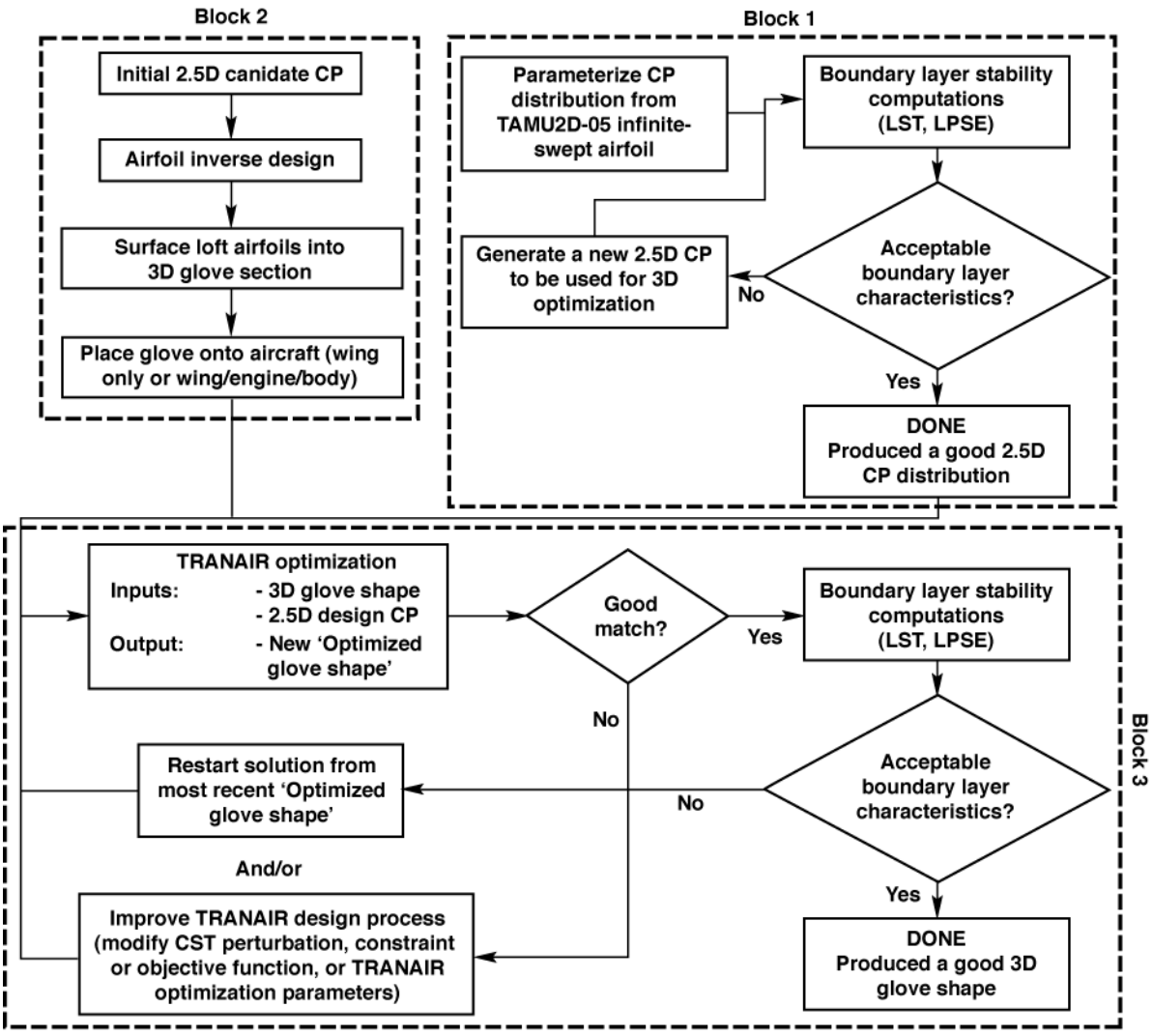

Figure 3. Glove optimization and design process.

A. Block One – Target Pressure Distribution and Boundary-Layer Stability

As seen in Fig. 3, one of the inputs to the 3D design process is a target pressure distribution. Throughout the design process, refinement of the target pressure distribution and the 3D optimization routine were run in parallel. Therefore there are multiple C_P distributions that are used in progressing stages of the 3D design process and thus presented in the results.

It is desired for the 3D glove test article to have a spanwise-invariant pressure distribution, particularly for available computational tools to be able to model the flow field and stability characteristics for validation studies. Here spanwise is assumed to be in the direction parallel to the LE. An infinite swept wing with its identical leading and trailing edge sweep angles Λ, infinite extent in span, constant airfoil cross-sections, and spanwise-invariant flow properties serves as an idealized, simpler model for the development of the target C_p distribution conducive to DRE control.

For an infinite swept wing, the spanwise component of the Navier-Stokes equations decouples from the components in the LE-normal plane. Thus, calculations can be simplified by being performed in 2D using the LE-normal component of the freestream velocity ($U_\infty = Q_\infty \cos \Lambda$) as the upstream boundary condition, and then solving and superposing the spanwise velocity component whose local edge inviscid value is constant ($W_\infty = Q_\infty \, sin \, \Lambda$). Because of the simplified modeling, the resulting pressure distribution will be termed the 2.5D pressure distribution.

The initial pressure distribution was parameterized and modified using B-splines. Since the boundary-layer solution and linear stability theory (LST) have negligible dependence on curvature, results were recomputed on the new pressure distribution while leaving the physical geometry unchanged. The TAMU2D-05 infinite-swept airfoil[1] was used here as the notional shape for the calculations.

As shown in Fig. 4, the parameterization only concerns the suction-side C_p forward of X/C ≈ 0.60, as this is the primary region of interest in the DRELFGE experiment, as well as the principal domain over which the optimizer operates. The philosophy of designing a pressure distribution for DRE control has been described previously.[1,3]

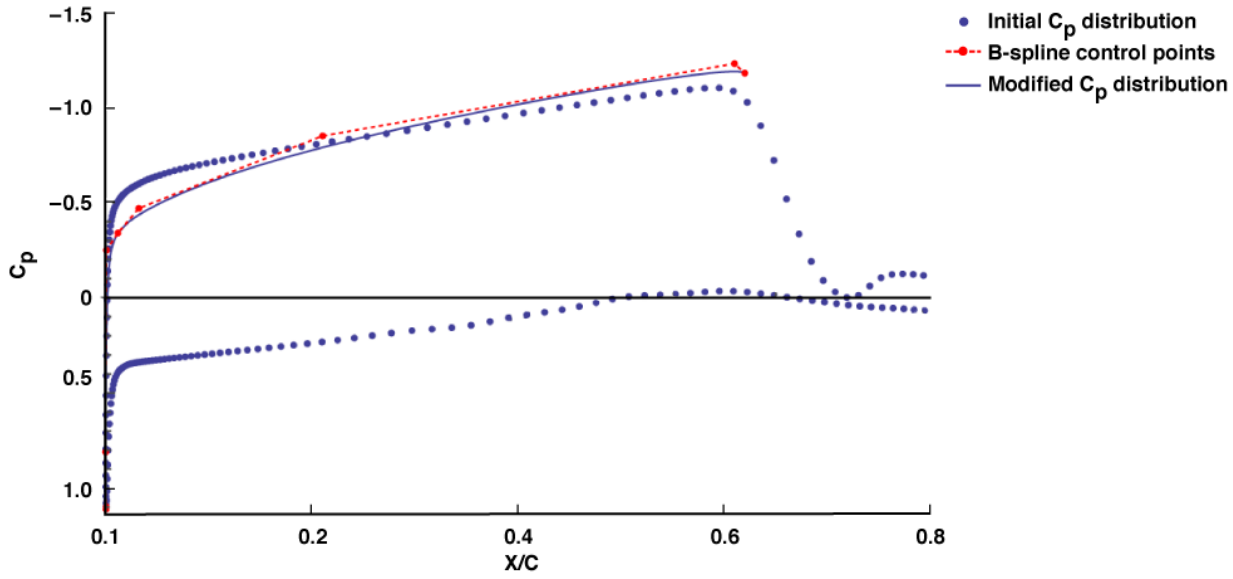

Figure 4. B-spline representation of the target pressure distribution (blue dots show the initial pressure distribution; red dashed line and dots are the control points of the B-spline function; blue solid line is the new target C_p distribution).

Two different approaches are being applied to determine the stability characteristics of a given pressure distribution and flow conditions: 1) linear stability theory (LST), a local normal-mode approach assuming parallel flow and no curvature, and 2) linear parabolized stability equations (LPSE), in which the evolution of disturbances is determined by a marching scheme including non-parallel and curvature effects. The tool LASTRAC[9] using an infinite-swept-wing boundary-layer solution from WINGBL,[2,10] a spectral boundary-layer solver for infinite swept wings, is used for both approaches. In the determination of the 2.5D target C_p, LST is used. The WINGBL2/LASTRAC LST calculations were verified internally against the Q3BL/LST3D code[11] and found to be in good agreement. LPSE is used for assessment of the final 3D glove design (see Section VI.D). Future work will also consider boundary-layer profiles obtained from a fully viscous Navier-Stokes computation on the full aircraft, which more completely accounts for spanwise non-uniformity in the boundary layer as well as the C_p.

The range of unstable frequencies and wavelengths considered was typically 1 kHz $\leq f \leq$ 10 kHz for a Tollmien-Schlichting (TS) wave normal to the LE (i.e., zero spanwise wavenumber) and 1 mm $\leq \lambda \leq$ 40 mm for stationary crossflow (CF) ($f = 0$). The experiment considers stability in two Reynolds number (Re_c) ranges: Re_c = 15–20 million for natural laminar flow (NLF) and Re_c > 22 million (nominally up to Re_c = 30 million) for DRE control. Based on prior experience, transition is assumed to occur under NLF conditions at $N = 14$ for a highly polished LE (≈ 0.3 micron RMS surface roughness) and at $N = 9$ for an "operational" surface roughness (≈3-4 micron RMS).

B. Block Two – Initial 3D Glove Design

Once the 2.5D target pressure distribution is created for nominal flight test conditions (Fig. 5), the initial 3D glove is designed. This process is briefly summarized as follows with the full design methodology described previously.[3]

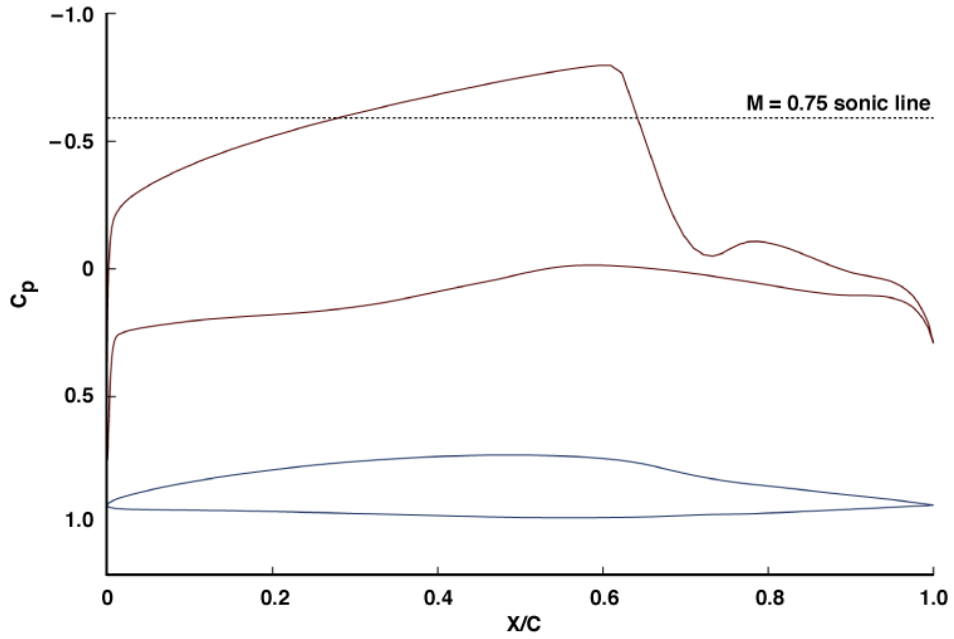

Figure 5. Optimized final target pressure distribution and notional 2D airfoil.

First, two 2.5D airfoils are generated: one meeting the target pressure distribution and GIII geometric constraints for the inboard section of the glove and the other for the outboard. That is, each of the two airfoils is generated separately assuming an infinite-swept-wing geometry and using an inverse method with a 2D implementation of the class-shape-transformation (CST) optimization process described in Section V.B.

Once the airfoils are created, the glove section is formed by linearly lofting a surface between the two airfoils. The glove section is placed onto a CAD model of the aircraft, and then faired back into the wing of the aircraft using inboard, outboard, and aft blends. When this initial 2.5D glove design is lofted into a 3D wing glove, an integration of fuselage, engine, and other 3D effects due to the wing geometry and the fairings affects the pressure distribution, and the target requirements are not met. To account for these factors and again meet the target pressure distribution, the 3D glove shape needs to be optimized. The process and the results of the 3D glove optimization are the main focus of this paper.

C. Block Three – Full 3D Glove Design and Optimization

The 3D design process begins with the optimization of the initial 3D wing glove using TRANAIR. TRANAIR is a non-linear full potential code directly coupled with an integral boundary layer model that contains an optimization algorithm. User defined inputs for the geometry perturbation, constraint, and objective functions were created for use in the TRANAIR optimization algorithm. The details of the optimization routine are contained in Section V.A. Optimization is not inherently a cut and dry process where one puts in a few inputs, and expects a perfect answer. Optimization requires the user to draw from existing knowledge to help make decisions such as choosing the best starting point for the optimization, designing the objective function, and choosing the correct constraints to obtain the best solution possible. This led to an evolutionary design process for the 3D glove shape, which is the main focus of the paper and is described in detail in Section VI. To begin the design cycle, the initial optimization problem was constructed and executed using the initial 3D glove design described in Section IV.B. The results were visually analyzed to determine the quality by comparing the target and glove pressure distributions to see how closely they matched, how wavy they were, and how spanwise uniform the flow over the glove was. If the results were not deemed acceptable, one of two methods to improve the design was attempted. The optimization problem was restarted from the result of the previous solution, which provided a better starting guess for the optimizer. Otherwise, the perturbation routine, constraint or objective functions, or the TRANAIR optimization parameters were modified and improved, and the optimization process was run again from the same initial starting point. If the results of the optimization passed visual inspection (described in Section VI), a streamwise slice of C_p is taken along a constant buttline section of the newly optimized glove test section. The boundary-layer profiles for this C_p slice are calculated by assuming a locally infinite swept wing, and the boundary layer stability is computed in the same manner as for the 2.5D pressure distribution described in Section IV.A. If the new optimized glove shape did not have the required stability characteristics to satisfy the DRE experiment, the optimization process is modified and started again. However, if the results showed the required characteristics, the design is then considered complete.

The 3D design started with the glove mounted on a wing-only model. This was a good starting point for the process because it helped to reduce the complexity of the grid, and reduce the solution time for an optimization cycle. Once a few

optimizations were attempted on the wing-only geometry, the nacelle and body were added to the geometry in order to capture the interference effects and the influence that the body and nacelle have on the local flow over the glove. The final results of the optimization process were obtained using the full wing/body/nacelle configuration.

V. Optimization Description

TRANAIR has a robust design optimization feature that allows constrained multi-point design that was developed at Boeing and used for many years as a design tool for their aircraft. TRANAIR allows user-defined movement, constraint and objective functions including inequality constraints.[12] The user-defined movement routine used is the CST routine, which allows for fewer design variables than a traditional mesh point optimization. There is an active two-inch clearance constraint that is imposed on the design so that the wing glove has two inches of room between the wing surface and the glove surface for the mounting devices. The initial objective function matches the target pressure coefficient (C_p) distribution at multiple locations across the span of the glove test section. The target pressure distribution used in the optimization is the same optimized 2.5D pressure distribution described in Section IV.A.

A. TRANAIR Optimization

TRANAIR has the capability to solve constrained aerodynamic design problems through the use of transpiration, which modifies the mass flow boundary conditions of the panels to approximate the surface movement. In the TRANAIR design algorithm, the aerodynamic analysis on each grid is solved first and then the flow sensitivities with respect to the design variables are generated. An optimization problem is then constructed based on user inputs of the design variables, constraints, and objectives. Constraints and objectives can either be flow or geometry based and are linearized with respect to the design variables. The constructed optimization problem is then sent through an optimizer that determines the values of the design variables that minimize the objective function while not violating the specified constraints. The geometry is then perturbed through transpiration using the user-defined movement routine. The updated geometry and design variables are then used in the adaptive grid refinement process in preparation of solving the flow on the next grid.[8] One inherent pitfall with the TRANAIR optimizer is that it uses a gradient-based line search method, which has difficulty distinguishing between a local and global minimum. The method attempted to avoid finding a local minimum in this process was to vary the values of the initial design variables to see if changes in the starting point yielded a different optimized glove shape. If the optimizer always converged to the same solution over a wide range of initial design variables, the solution is most likely a global minimum.

B. CST Design Method

The CST routine invented by Kulfan[13,14] is used to provide a mathematical description of a geometry through a generalized class function definition, with a series of shape functions to further define the geometry. The class function is a generalized equation that allows for the creation of a wide variety of geometries. The shape function is a simple analytic function that controls the design parameters with only a few scalable values. The CST method is very powerful in its ability to model both 2D and 3D shapes efficiently with as few design variables as possible. Because of its ability to model a wide variety of shapes, including an oddly shaped wing glove, along with the computational time savings associated with fewer design variables, the CST method was implemented as the perturbation routine for the optimization algorithm.

The CST method, created by Kulfan is nicely summarized by Lane,[15] and is reproduced here for reference. The general form of the CST method is based on Bezier curves with an added class function which takes the general form seen in Eq. (1),

$$\zeta_i(\psi) = C_{N2}^{N1}(\psi) \cdot S_i(\psi) \tag{1}$$

where C and S represent the class and shape functions respectively. Ψ equals the non-dimensionalized X coordinates (X/C). The class function is defined in Eq. (2),

$$C_{N2}^{N1}(\psi) = \psi^{N1} \cdot (1-\psi)^{N2} \tag{2}$$

where exponents $N1$ and $N2$ define a variety of general classes of geometries. For classic National Advisory Committee for Aeronautics (NACA) four series symmetrical airfoils, the $N1$ and $N2$ factors are 0.5 and 1.0 respectively. Since this paper focuses on a wing glove, the factors of 0.5 and 1.0 will be used throughout the design process. The shape function modifies the profile obtained by the class function and is represented by a Bernstein polynomial as shown in Eq. (3),

$$S_i(\psi) = K_i^n \cdot \psi^i \cdot (1-\psi)^{n-i} \tag{3}$$

where n is the order of the Bernstein polynomial and K is the binomial coefficient which is defined in Eq. (4) as

$$K_i^n = \frac{n!}{i!(n-i)!} \tag{4}$$

The class and shape functions are then superimposed to produce a 2D CST curve seen in Eq. (5),

$$\zeta(\psi) = \sum_{i=0}^{n} A_i \cdot \zeta_i(\psi) \tag{5}$$

A is the array of design variables that are defined through the optimization process. To expand the CST method to a 3D geometry, the shape functions now takes the form in Eq. (6) as per Mousavi,[16]

$$S_i(\psi, \eta) = B_{i,j} \cdot Sx_i(\psi) \cdot Sy_j(\eta) \tag{6}$$

where η = Y/C is the non-dimensional spanwise length and Sy is the shape function in the spanwise direction. The surface of the wing is now defined by Eq. (7),

$$\zeta(\psi, \eta) = \sum_{j=0}^{ny} \sum_{i=0}^{nx} A_{i,j} \cdot C_{1.0}^{0.5} \cdot S_i(\psi, \eta) \tag{7}$$

In the design problem, the wing X and Z coordinates are perturbed as seen in Eqs. (8a) and (8b),

$$\Delta x = \frac{x}{c} * \zeta(\psi, \eta) * C_{local} \tag{8a}$$

$$\Delta z = \frac{z}{c} * \zeta(\psi, \eta) * C_{local} \tag{8b}$$

This CST method is the main perturbation routine used in the optimization process. In addition to the CST method, the glove is allowed to twist linearly from the inboard to outboard portions of the glove about the quarter chord. The perturbation routine also allows for the local chord length of the glove to change. The length change is just a simple scaling of the X coordinates to shrink or grow the glove forward of the aircraft 60% chord line.

The original design of the glove is comprised of the test section, which is blended back in with the wing by creating inboard and outboard fairings to continuously blend the sides of the test section, and a continuous blend that connects the trailing edge (TE) of the test section to the wing. The edges of the glove that intersect the wing surface are not allowed to move in the optimization routine to maintain continuity between the glove and the wing surface. However, the amount the fairings are allowed to be perturbed varies bi-cubically from zero at the wing intersection to 1 (full movement) at the test section intersection. This allows for the fairings and blending regions to maintain a nice smooth blend from the wing surface into the glove test section, while allowing them to be partially optimized.

C. Constraint and Objective Functions

The initial objective function for the optimization process is a common pressure matching routine. Throughout the optimization process the routine was modified, and the changes will be explained in Section VI. The current 2.5D C_p is used as the objective function at multiple span stations on the test section. The original objective function is written as a panel area weighted least squares fit seen in Eq. (9),

$$Obj_1 = Abs\left(\frac{Dx}{10}\right) * \left(C_p - C_{pt}\right)^2 \tag{9}$$

where Dx is the panel length in the X direction, C_p is the current computed pressure coefficient at the node, and C_{pt} is the target pressure coefficient at the node. This equation is applied at every node on the given wing slice and summed up to create one objective function value per wing slice.

The constraint function is a simple algorithm that ensures that the 2-in clearance from the wing is maintained where necessary, and a 0-in constraint is maintained everywhere else for the glove. The 2-in clearance on parts of the glove is necessary to leave room for the mounting system. The 0-in clearance is necessary everywhere else because the glove cannot physically protrude into the wing. Referencing Fig. 1, the 2-in clearance constraint is imposed on the test section (blue), and the 0-in constraint is imposed on the fairings and TE blend (red and green). Seven nodes on each span slice are used as constraints that are spread out over each airfoil section to ensure the necessary clearances are maintained everywhere.

VI. 3D Optimization Results and Discussions

Any optimization problem is a learning process where the user sets up and runs an optimization, and then makes a learned decision to change the objectives, constraints, and design variables. This cycle is repeated as many times as needed to develop the best optimization setup for the specific problem. The results presented will be a reflection of the learning process and will help the reader understand the work and the effects of different approaches to the problem.

A. Target Pressure Distribution

There were a total of three target pressure distributions that were used throughout the 3D design process. As the 3D design process progressed, so too did the 2.5D target C_p process. The final target pressure distribution is shown in Fig. 5. The pressure distribution achieves the target section C_l = 0.5 at the design M = 0.75. A representative calculation of LST N-factors in Fig. 6 shows that the NLF requirements are nominally achieved by the target C_p distribution. In Figure 6, stationary crossflow N factors first pass through the notional limit of N = 14 around X/C = 0.52, which signifies that transition is expected to occur at that chord location for a highly polished LE, triggered by the most-unstable LE-parallel wavelength of 10 mm. Streamwise instability in the LE-normal direction was calculated to be negligible.

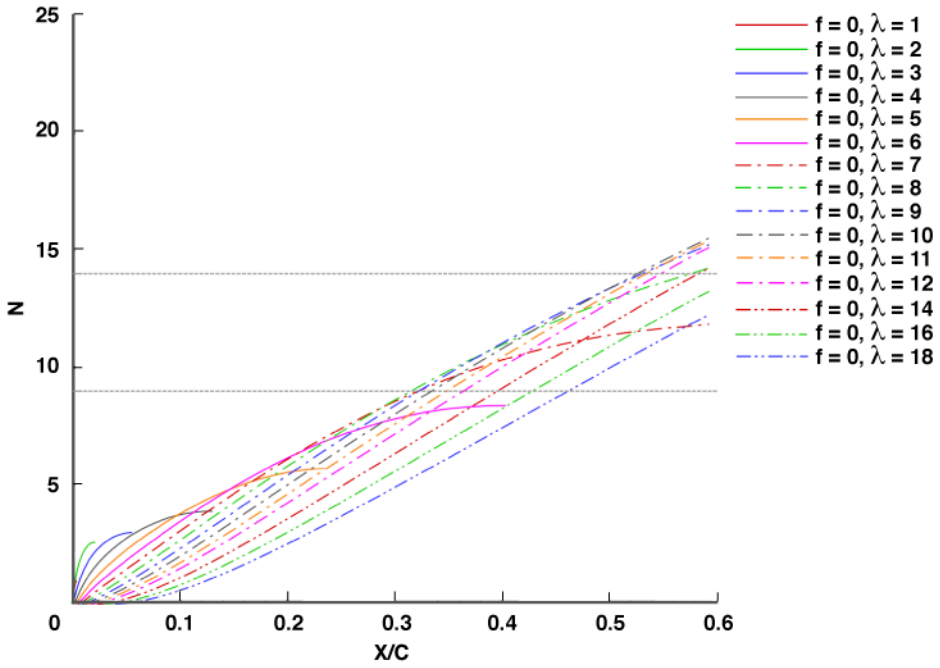

Figure 6. Target C_p LST N-factors in NLF regime: M = 0.75; Re_c = 17.5 million (c = 4.4 m, H = 43,610 ft). Dashed horizontal lines show expected transition N-factors for polished (N_{tr} = 14) and operational (N_{tr} = 9) LE roughness. Spanwise wavelengths are in mm.

In the DRE range at Re_c = 22 million, shown by the LST N-factors in Fig. 7, transition is expected at approximately X/C = 0.4 for a highly polished LE because that is when the most unstable LE-parallel wavelength of 8-9 mm reaches N = 14. A spanwise wavelength of 4 mm is a viable candidate for DRE control spacing to stabilize the most unstable wavelength of 8-9 mm. DREs can be expected to delay transition back to at least X/C = 0.60 in this case. At Re_c = 30 million, expected transition moves forward to X/C = 0.32, while 3 mm is a candidate control wavelength.

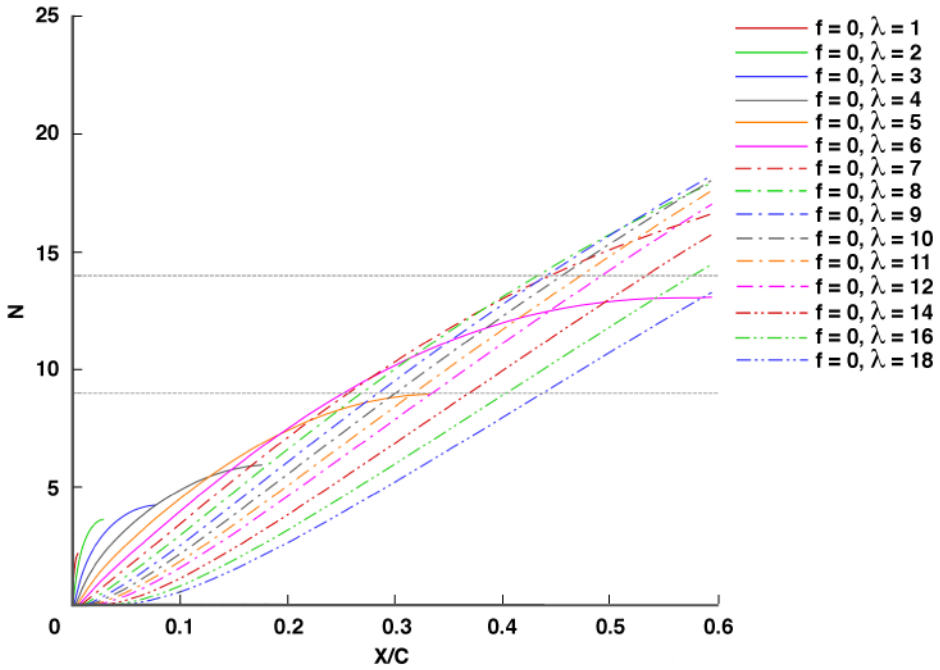

Figure 7. Target C_p LST N-factors in DRE regime: M = 0.75; Re_c = 22 million (c = 4.4 m, H = 43,610 ft). Dashed horizontal lines show expected transition N-factors for polished (N_{tr} = 14) and operational (N_{tr} = 9) LE roughness. Spanwise wavelengths are in mm.

B. Wing Only Results

To begin the 3D optimization process, the initial glove geometry is run through the TRANAIR optimizer without any geometry constraints. This first optimization run is termed design run 1 (DR1) and is completed to see ideally how the optimizer wants to perturb the wing glove when there are no restrictions imposed upon it. Additionally, there is no length change allowed in the initial design routine. Twelfth order chordwise Bernstein polynomials (n = 12 in Eq. (3)) are used for both the upper and lower surfaces for the CST method. Referencing back to Fig. 3, the next step in the 3D design cycle is to visually inspect the optimized glove shape to help ascertain the quality of the optimization. A comparison between the original glove and the initially optimized glove is made using the center span section of the wing glove in Fig. 8. The resulting optimized glove shape from DR1 has a decreased height on the upper surface in order to reduce the pressure peak on the aft region of the glove.

Figure 8. Comparison of the original and DR1 glove using the center span section (original shown in green; DR1 shown in red).

Figure 9 (left) shows the pressure distributions for the un-optimized test section at three span stations and Fig. 9 (right) shows the resulting pressure distributions from DR1 compared to the target C_p.

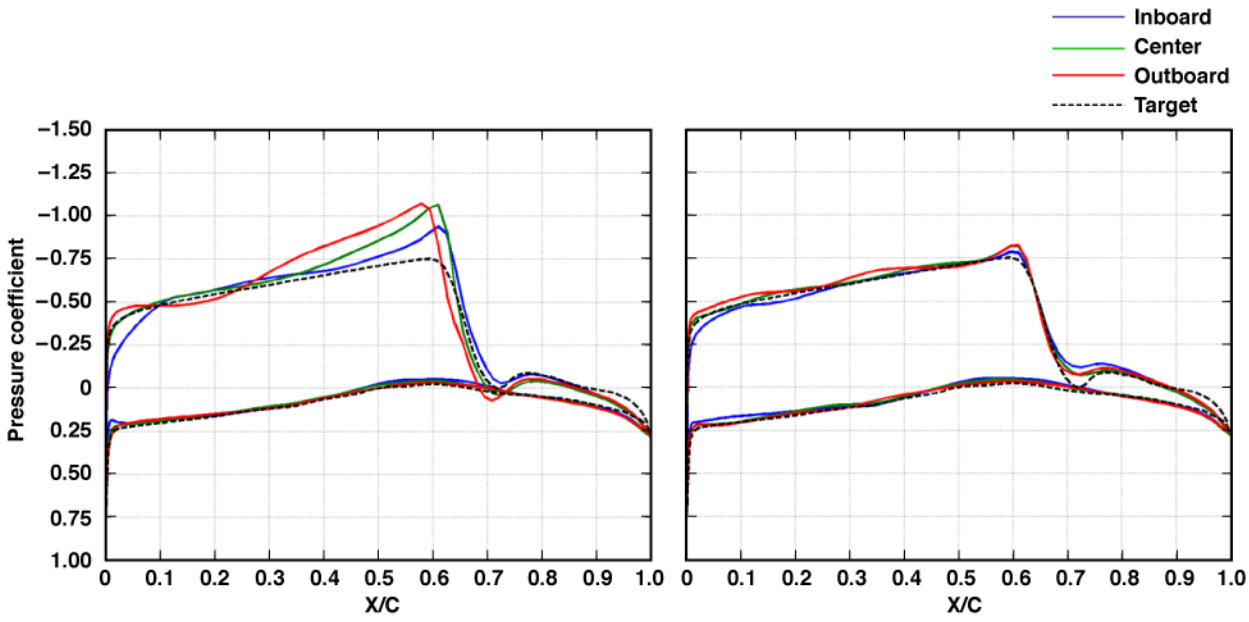

Figure 9. Pressure distributions across three sections of the wing glove. Left: un-optimized glove. Right: DR1.

Figure 9 (left) shows the pressure distributions across the un-optimized glove are not uniform in the span direction. Flow near the LE of the wing glove on the outboard and inboard sections has very different C_p values, slope, and curvature compared to the target pressure distribution. Additionally, there is a very large pressure peak near 0.60 X/C across the entire glove, which creates a large disturbance in the flow and reduces the extent of laminar flow seen over the wing glove. The large differences between the actual pressure distributions and the target validate the need to optimize the glove shape in 3D to increase the laminar flow capability.

Compared to the initial un-optimized glove design, Fig. 9 (right) shows that the modified glove C_p distributions from DR1 are much closer in shape to the target 2.5D C_p. Even though closer, it appears that the optimizer weights the aft sections of the upper surface much more than the LE section because of the panel area weighting in the objective function. This is apparent in Fig. 9 (right) because of how well the optimizer matches the target C_p between X/C = 0.20 and 0.60, and how poorly it matches between the target and C_p distributions near the LE. It is very important to have a good pressure distribution on the upper surface, but for tailoring a wing surface to have specific stability characteristics, the LE is the most critical. Otherwise, the major problem with this first optimization run is that the upper surface of the glove has less than 2-in of clearance to the wing surface because no geometry constraints are added.

Since the results from DR1 do not pass visual inspection, the optimization parameters will be modified and the optimizer will be run again from the same initial glove geometry. For the next design run (DR2), the panel area weighting was reduced in an effort to reduce the error of the pressure matching near the LE. Additionally, the length of the glove is treated as a design variable with a limit set for the maximum extension in front of the glove. However, the 2-in clearance constraint is still not satisfied in DR2, which has to be included in the next optimization. With the clearance constraints added into the optimization problem (DR3), the resulting optimized glove has the required amount of clearance from the wing allowing space for the glove attachment mounts. The resulting pressure distributions for DR2 and DR3 can be seen in Fig. 10 (left) and Fig. 10 (right) respectively.

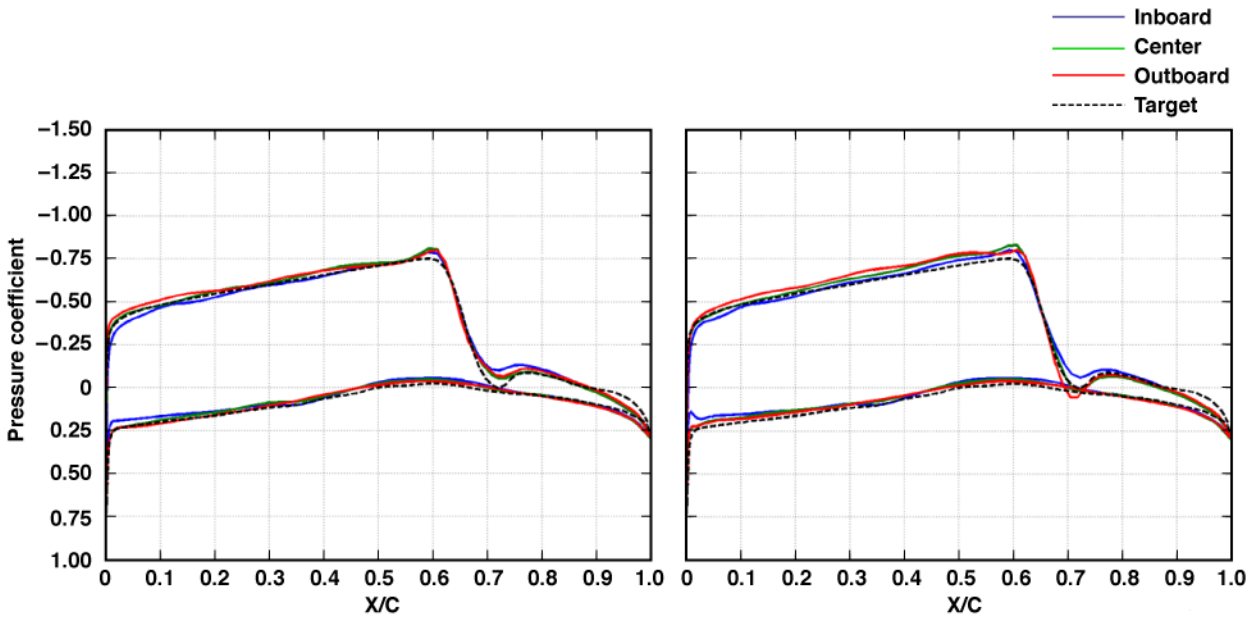

Figure 10. Pressure distributions across three sections of the wing glove. Left: DR2. Right: DR3.

Reducing the panel area weighting and allowing the wing glove to shrink in length, shows a slightly better pressure matching to the target distribution, although the shape of the optimized geometry does not change significantly from the optimized geometry with no clearance constraints. With the constraints added in DR3, instead of reducing the thickness of the upper surface, the optimizer added twist to the wing glove, and also reduced the total aircraft angle of attack. These changes that the optimization made allowed for the clearance constraints to be satisfied while maintaining a close match to the target pressure distribution, similar to that of DR2.

The pressure distributions in Fig. 10 (right) from DR3 are very close to a finely optimized glove. However, waviness in the geometry, which is apparent in the C_p distribution, is produced by the perturbation routine that needs to be smoothed out before the design is considered to be acceptable. The next attempt to smooth out the glove (DR4) consisted of making two changes to the optimizer: increase the order of chordwise CST to $n = 24$, and also to not require the optimizer to match the pressure distribution on the glove TE blending region. It is evident in the C_p results of DR4, seen in Fig. 11 (left), that increasing the order of the CST helps to reduce waviness at the inboard and center locations because the C_p distributions at those sections are much smoother. Additionally, not requiring the optimizer to match the blending region works to reduce the pressure peak seen around X/C = 0.60.

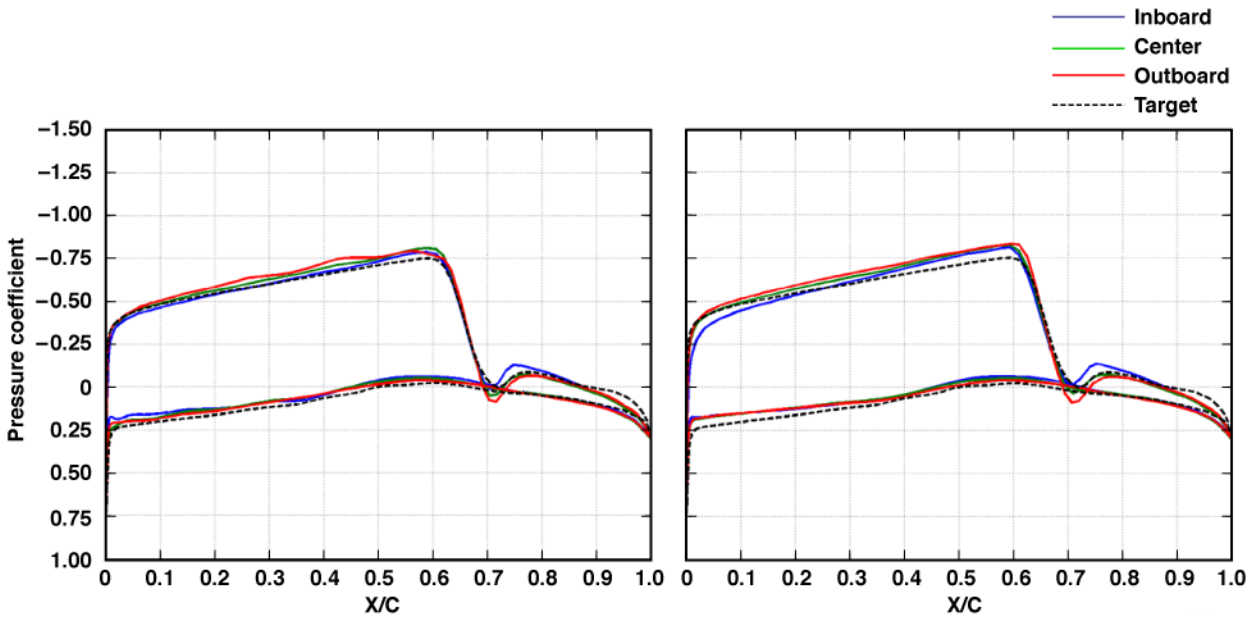

Figure 11. Pressure distributions across three sections of the wing glove. Left: DR4. Right: DR5.

In an attempt to reduce the waviness further, the objective function was modified from only matching the C_p values to also matching the slope of the C_p distribution. This new addition to the objective function is normalized because the slope can vary from infinity at the LE to zero around X/C = 0.60. This modification is critical, as it will be shown shortly that matching the slope of the C_p is important when it comes to preserving the stability characteristics of the target C_p. Equation (10) shows the new portion added to the objective function.

$$Obj_2 = Abs\left(\frac{Dx}{10}\right) * \left(\frac{\left(C_{p_{slope}} - C_{pt_{slope}}\right)}{C_{pt_{slope}}}\right)^2 \tag{10}$$

Since the objective function is now compromised of two discrete functions, they need to be combined so that the optimizer only needs to find the minimum of one function. This is done by finding the weighted sum of the two functions. This method gives the user the flexibility to determine which individual function will most affect the final design. A ratio of 10:1 between the C_p value matching and the slope matching was chosen as the initial weighting of the two functions. This ratio resulted in the weighted sum of the objective function as shown in Eq. (11),

$$Obj = 10 * Obj_1 + 1 * Obj_2 \tag{11}$$

where Obj_1 is the C_p value matching function (Eq. (9)), Obj_2 is the C_p slope matching function (Eq. (10)), and Obj is the weighted sum of these two functions. The waviness in the optimized solution was greatly reduced by applying this new objective function to the same optimization parameters used in design run four. With this improvement to the optimization algorithm, the initial glove shape was optimized again (DR5). The resulting C_p distributions on the optimized glove shape are shown in Fig. 11 (right).

The addition of the slope matching routine drastically reduced the waviness of the C_p distributions on the glove, which indicate the reduction of waviness of the glove geometry. However, as a result of the optimizer trying to match the slope, it is apparent in Fig. 11 that the glove pressure distributions do not match that of the target C_p distribution as accurately as DR4. Similar to the slope matching objective function, a third objective function that tries to match curvature of the target C_p, was considered, but was not found to have a significant effect on the optimization results. Higher order chordwise CST ($n > 24$) was also attempted to look for an improvement in the C_p matching. However, there was significant round off error because of the factorials seen in Eq. (4) of the CST formulation. The factorial of 24 ($24! = 6.2045 \times 10^{23}$) is very large and unfortunately anything higher than $n = 24$ cannot be handled without significant error in TRANAIR.

Currently in the optimization process (DR5), the geometry perturbation function utilizes $n = 24$ order CST curves, maintains the required clearance constraints across the glove, and uses an objective function that is the weighted sum of the C_p value and C_p slope matching. These same optimization parameters were applied with a new intermediate target C_p and a new optimization cycle was run (DR6). The optimized glove pressure distribution comparison is seen in Fig. 12. Part of the objective with this new target C_p was to test the ability of the optimizer to match distributions with varying characteristics. In comparison to the previous C_p, this C_p has a lower pressure minimum, which implies a larger region of supersonic flow.

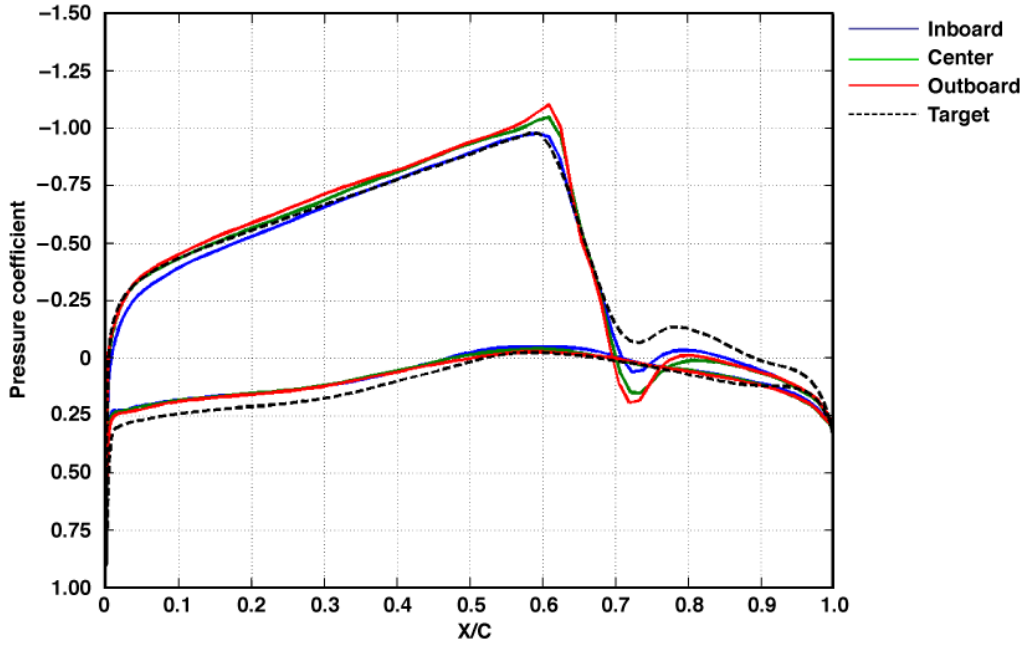

Figure 12. Pressure distributions across three sections of the wing glove DR6.

Even though Fig. 12 shows qualitatively decent matching at the center and outboard span stations, there are still some discrepancies between the target and the resulting glove pressure distributions that may be improved upon. The pressure peak at X/C = 0.60 can be reduced, the inboard section could match the target better, and the overall spanwise uniformity can be improved upon. There are a certain number of iterations specified to converge to an optimum in any given TRANAIR design run. If the starting geometry has a pressure distribution that is very different than the target, many of these iterations will be used to drastically change the geometry, and only a few are left to fine tune the design. Even if one increases the number of iterations, the optimizer can get bogged down when it is getting close to the minimum. It follows then that starting from a geometry that yields a pressure distribution close to the target will produce a better final design. In this manner, the objective function is re-scaled, so the steps that the optimizer takes to get to the final solution are less. Referencing Fig. 3 in this scenario, since the optimized glove did not pass the visual inspection, instead of improving the optimization parameters, the optimized glove shape from DR6 will be used as the input geometry to a new TRANAIR optimization run known as DR7. To better determine the benefit of starting from a closer-to-optimum point, this process was repeated two more times (DR8). Figure 13 (left) shows design runs 7 and Fig. 13 (right) shows design run 8.

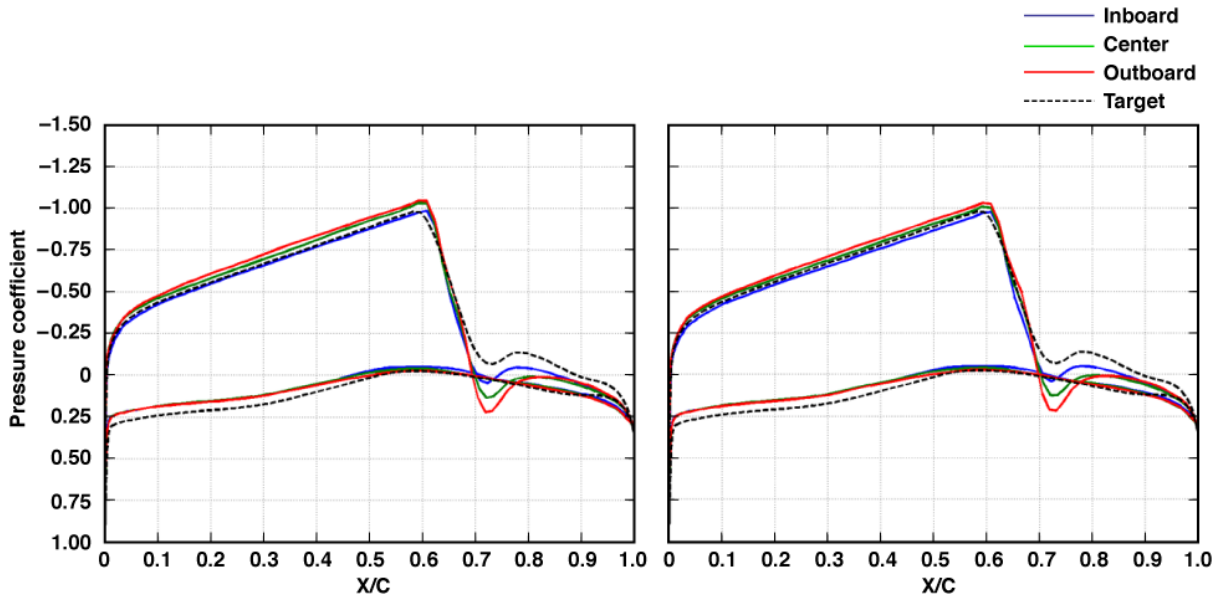

Figure 13. Pressure distributions across three sections of the wing glove. Left: DR7. Right: DR8.

Restarting the optimization routine from an optimized solution has a very beneficial effect. The pressure distributions match much more closely near the LE region and the spike at 0.60 X/C is virtually eliminated. However, in comparing Fig. 13 (left) and Fig. 13 (right), it can be seen that the changes between the two are minimal, which show that the benefit of restarting from an optimized solution plateaus after iterating through that method multiple times.

A good optimization routine has been developed using the experience gained through multiple design cycles using the wing-only geometry. The next step in the design and optimization process of the new wing glove will be to apply the same optimization routine to the glove when it is mounted on the wing/body/engine configuration.

C. Wing/Body/Engine Results

All of the results previously shown were computed on a model consisting of only a wing on a symmetry plane. The body and the engine are added in order to capture the interference effects and also the engine influence over the wing and glove. The same optimization parameters as DR7 were used but with the wing/body/engine geometry which produced the pressure distributions in Fig. 14 (DR9). This design run utilizes $n = 24$ order CST curves, maintains the required clearance constraints across the glove, and uses an objective function that is the weighted sum of the C_p value and C_p slope matching. The glove is run through the optimizer twice, using the initial glove design the first time, and the resulting glove shape of the first optimization run for the second run.

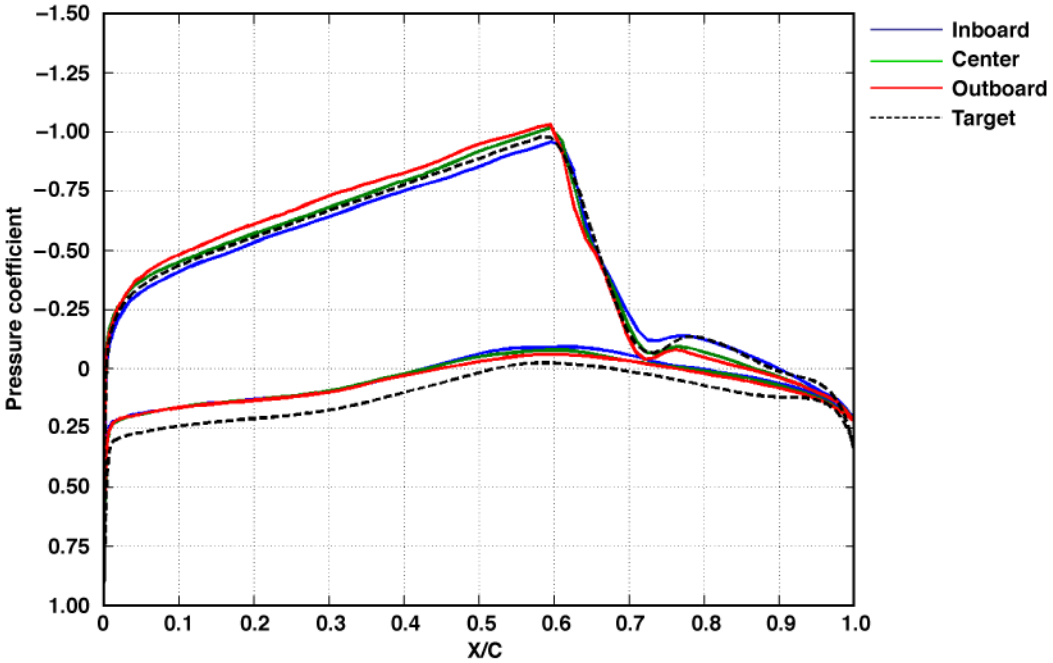

Figure 14. Pressure distributions across three sections of the wing glove DR9.

The resulting pressure distributions from the optimization look similar to those without the engine and body. The major difference is that the pressure side is more offset from the target C_p distribution. The offset, however, is not a fault of the optimizer, but rather, having the wing attached to the body changes the flow on the lower surface of the wing significantly. Given the constraints, and the objectives, the optimizer cannot possibly remediate the offset seen on the pressure side without sacrificing the pressure matching on the suction side. If one were to ignore the limitations, there are ways that the optimizer would try to better match target C_p on the lower surface. The first would be to reduce the thickness of the lower surface of the glove, which is not allowable because of the clearance constraints imposed. The second option would be to increase angle of attack, which would increase the C_p values on the pressure side. This would decrease the C_p over the upper surface of the glove, which would move the C_p distribution further away from the optimum. Even though the C_p offset exists and would be hard to reduce, stability results show that the C_p offset on the pressure side does not adversely impact meeting the experimental objectives. However, the pressure gradient still has to be favorable in order to maintain the possibility of laminar flow, as an adverse pressure gradient generally triggers transition due to TS (streamwise) instability.[17]

The new and final C_p distribution seen in Fig. 5 was introduced at this stage of the design process. The final C_p was used in the optimization process using the same parameters as DR9 except it used 18th order CST curves ($n = 18$) instead of 24th order. The C_p results of this new design (DR10) can be seen in Fig. 15 (left). With the new target C_p, the pressure distribution near the LE of the glove does not match the target very well. To help improve the matching at the LE, the panel area weighting in the objective function was removed so that the LE would be weighted just as highly as everywhere else.

The resulting C_p distributions of this latest design run (DR11) are shown in Fig. 15 (right). Both DR10 and DR11 were run through three TRANAIR optimizations to obtain a better optimized glove.

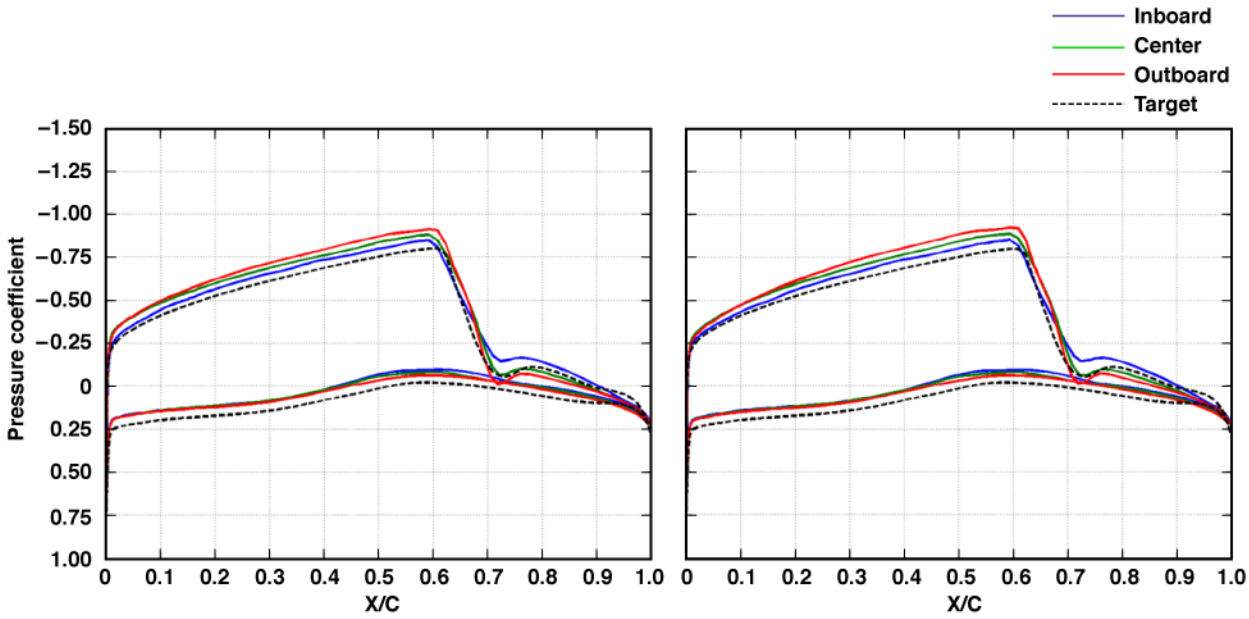

Figure 15. Pressure distributions across three sections of the wing glove. Left: DR10. Right: DR11.

By comparing the C_p results in Fig. 15 (left) and (right), it becomes apparent that removing the panel area weighting from the optimization seemed to improve the matching near the LE of the glove. Design runs 10 and 11 were run using 18th order CST (n = 18) to reduce computation time while maintaining accuracy. However, a comparison between 24th order and 18th order CST curves needs to be made to quantitatively determine which order of curves is the best to use for the final optimization of the glove. Using the parameters from DR11 (clearance constraints imposed, weighted C_p value, and slope matching objective function with no panel area weighting), the glove was run through eight optimization cycles using 18th order CST (DR12) with the C_p results seen in Fig. 16 (left). Separately, the glove was run through five design cycles using 24th order CST (DR13) with the C_p results seen in Fig. 16 (right).

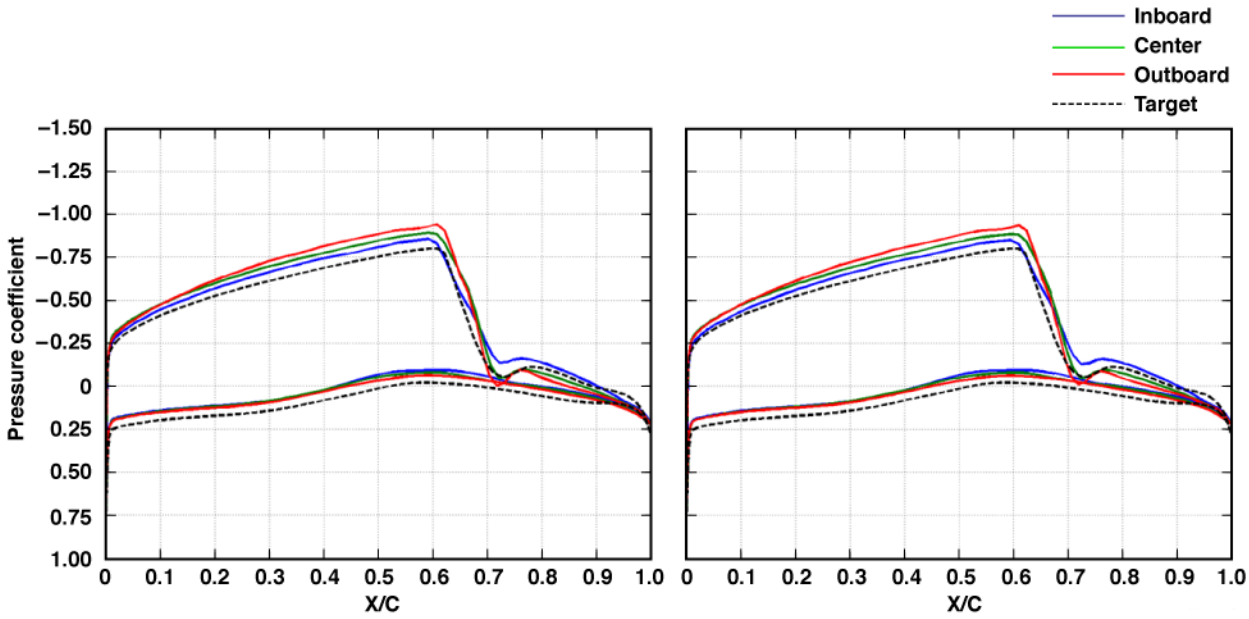

Figure 16. Pressure distributions across three sections of the wing glove. Left: DR12. Right: DR13.

Visually, the pressure distributions look very similar, with some minor differences. Therefore, following the flow chart in Fig. 3, the boundary-layer stability computations are performed to further evaluate the quality of the optimization. The optimization using chordwise 24th order CST (DR13) showed more promising stability and transition characteristics (but not acceptable for the final design) and was chosen as the launching point for the next set of optimization refinements. Even though the 18th order CST greatly reduces computation time, the accuracy of the 24th order CST geometry perturbation outweighs the benefit of running more optimization cycles with only 18th order CST.

A few additional modifications to the perturbation and objective functions were implemented in an attempt to further refine the design. The order of the spanwise CST curves was increased from five to seven in the span shape function in order to give the optimizer more flexibility. When using 24th order chordwise CST, the change from 5th to 7th order spanwise increases the number of design variables from 120 to 168, which significantly increases the computational time, but is acceptable in order to create a more accurate final design. The objective function was also modified to match the 2.5D C_p distribution at five different span stations instead of only three. This helped to further increase spanwise uniformity across the glove. Another modification to the objective function was to increase the weighting of the C_p value and slope matching on the upper surface compared to the lower. This worked to improve the C_p matching on the upper surface, while sacrificing the lower surface by a small amount. This was deemed an acceptable approach because the suction side of the glove is the most critical portion for the experiment. All of these modifications were combined with the lessons learned from the previous design into design run 14, and the pressure results can be seen in Fig. 17 (left). DR14 was run through six more optimization cycles to produce a more converged optimized glove (DR15), seen in Fig. 17 (right).

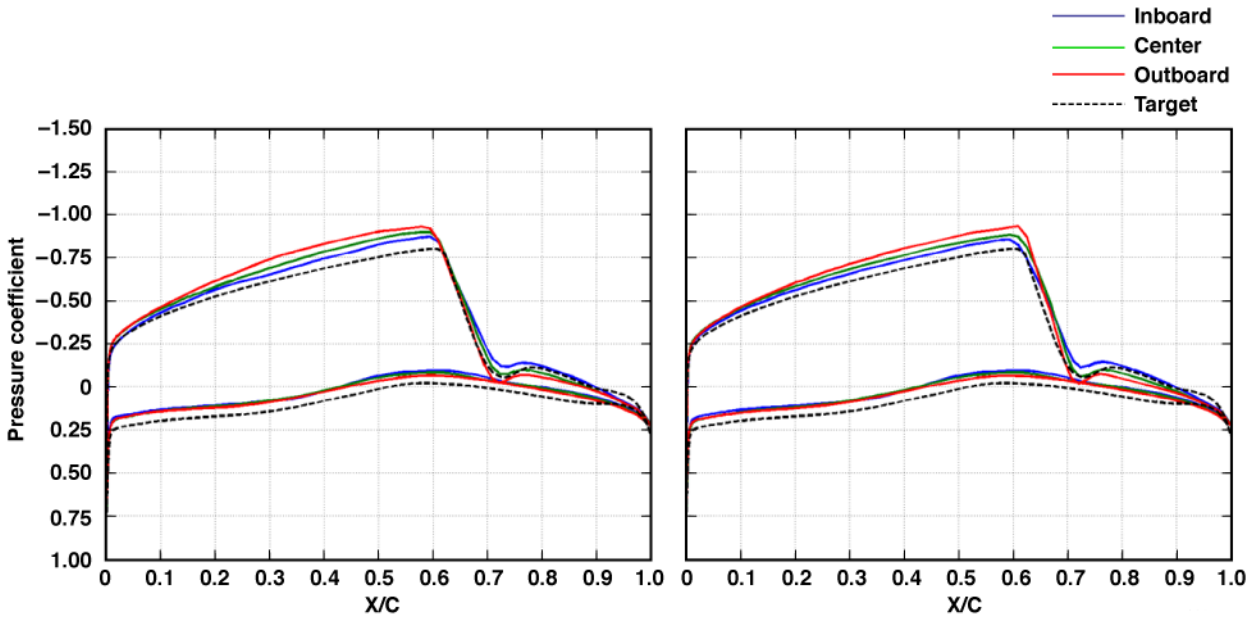

Figure 17. Pressure distributions across three sections of the wing glove. Left: DR14. Right: DR15.

The C_p distributions on DR15 look very similar to those on previous optimization attempts such as DR12 and DR13. So visual inspection can no longer be relied upon and therefore the boundary layer stability properties need to be computed for an accurate evaluation of DR15. The boundary layer properties generated from the stability results from DR15 are much better than those from any of the previous designs. However, all of the optimizations with the wing/body/engine configuration thus far consider a fully turbulent boundary layer on the glove, a choice made during the initial analysis for simplicity. Since the purpose of the glove is to produce laminar flow, the final glove shape needs to be designed to match the target C_p distribution with a laminar boundary layer, not a turbulent one.

An analysis run was performed on the optimized glove shape resulting from DR15, but using a laminar boundary layer across the glove seen in Fig. 18 (left). This resulted in a large pressure peak slightly past 0.60 X/C across the glove.

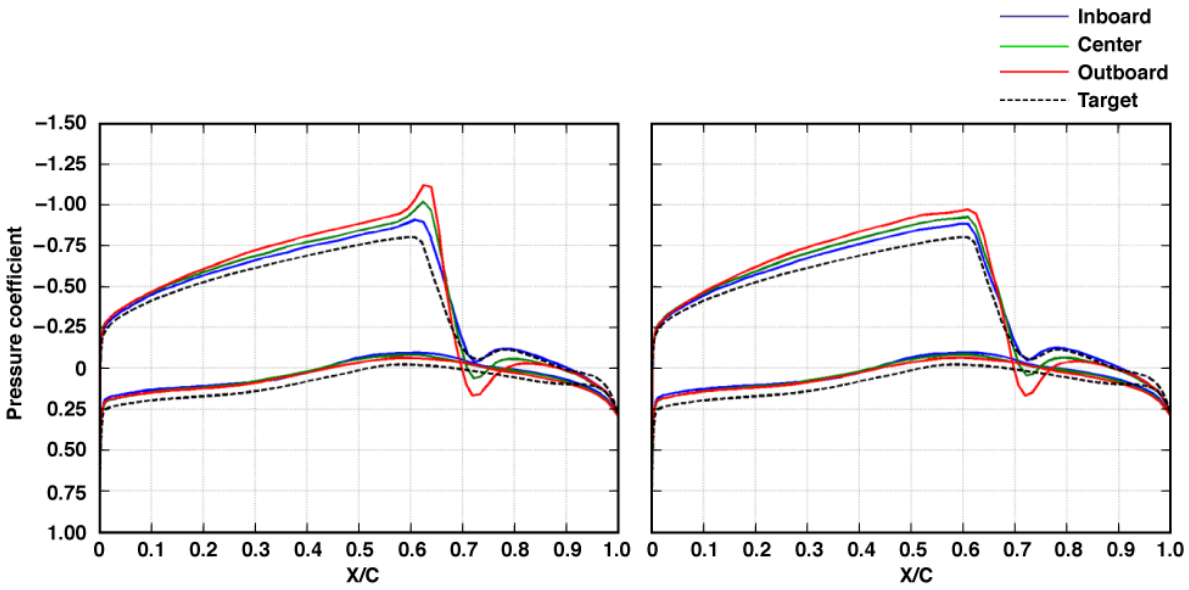

Figure 18. Pressure distributions across three sections of the wing glove. Left: DR15-lam. Right: DR16.

The pressure peak shown in Fig. 18 (left) is not acceptable for the design of the glove. Therefore, the optimized glove shape geometry from DR15 is used as the input for a TRANAIR optimization cycle using a laminar boundary layer (DR16) with the results seen in Fig. 18 (right). Design run 16 worked well to reduce the pressure peak from the laminar result of DR15. However, in reducing the peak, the optimizer increased the distance between the glove pressure distributions and the target. This difference is evident in when one compares the C_p distributions for DR16 in Fig. 18 (right). Additionally, the C_p distribution in Fig. 18 (right) is wavy, which shows that the optimized glove shape from DR16 is wavier than would be ideal. Because of time constraints on the project, the optimized glove shape from DR16 was used as an input to the beginning of three more TRANAIR optimization cycles. The weight of the C_p slope matching was also increased for these three extra optimization cycles in an effort to reduce the waviness seen on the glove. The resulting final glove design shows boundary layer stability results that enable a good DRE experiment when run through LST and LPSE computations as described in Section VI.D.

Figure 19 (left) shows the C_p distribution on the original glove design, and Fig. 19 (right) shows the C_p distribution on the final optimized glove design. Comparing these C_p distributions show that the optimization process greatly increased the spanwise uniformity of the flow over the glove. Figures 20-22 show a geometry comparison between the initial and final glove design at the inboard, center, and outboard cross sections of the glove.

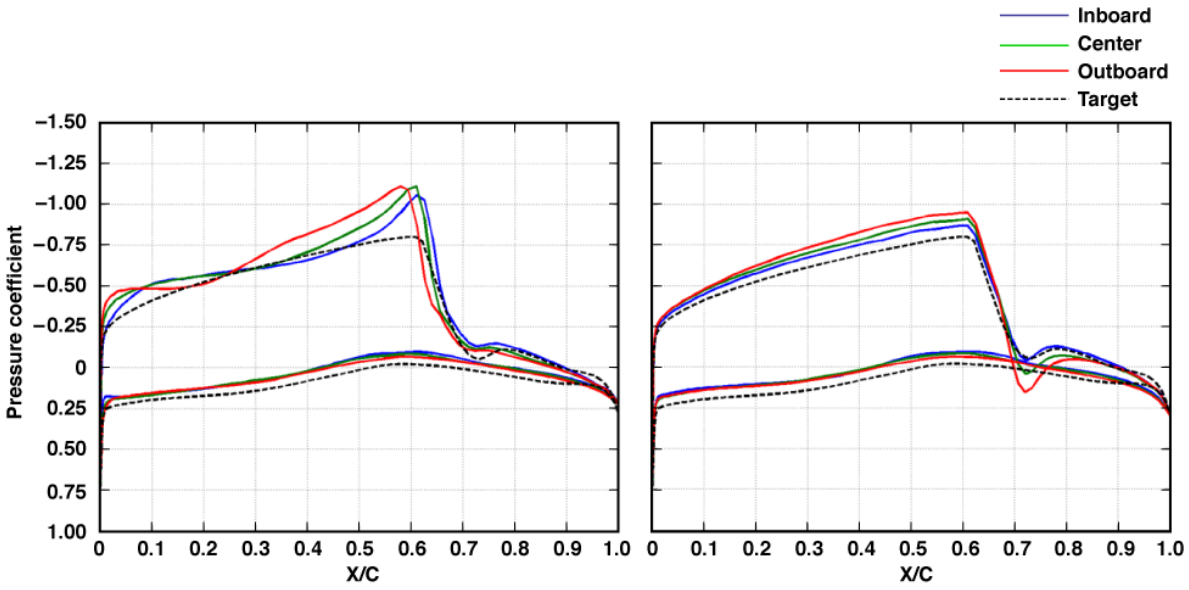

Figure 19. Pressure distributions across three sections of the wing glove. Left: original glove. Right: final optimized glove.

Figure 20. Comparison of the original and final optimized glove at the inboard span section (original shown in green; optimized shown in red).

Figure 21. Comparison of the original and final optimized glove at the center span section (original shown in green; optimized shown in red).

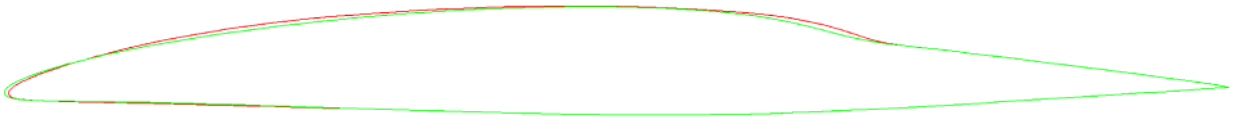

Figure 22. Comparison of the original and final optimized glove at the outboard span section (original shown in green; optimized shown in red).

The overall shape of the optimized glove never varied by more than one inch from the original shape, which highlights the sensitivity of the C_p distribution in this Mach range to small variations in geometry. Seen in Figs. 20-22, the optimizer changes the entire shape and camber of the glove, and also increases the washout. Furthermore, the laminar stability characteristics will be very sensitive to the C_p shape, which further highlights the need for this optimization.

D. Boundary-layer Stability Analysis

The stability results confirm the validity of the newly optimized gloved design. Figure 23 shows a comparison of LST *N*-factors at BL234 with the target-C_p *N*-factors from Figure 7. The optimized results show that the LST *N*-factors compare favorably with the target-C_p *N*-factors. Even though the optimized C_p profiles are offset from the target C_p, the important feature to note is that the C_p slope is matched consistently across the glove span, which leads to similar stability characteristics observed across the entire span of the glove. An assessment showing LPSE results is shown in Fig. 24. In contrast to the un-optimized glove design,[3,18] the LPSE N-factors are very similar to the LST computed N-factors. Since LPSE includes both curvature and non-parallel effects and LST does not, this leads to the conclusion that potentially excessive stabilization due to curvature does not appear to be a concern in the final optimized glove design.

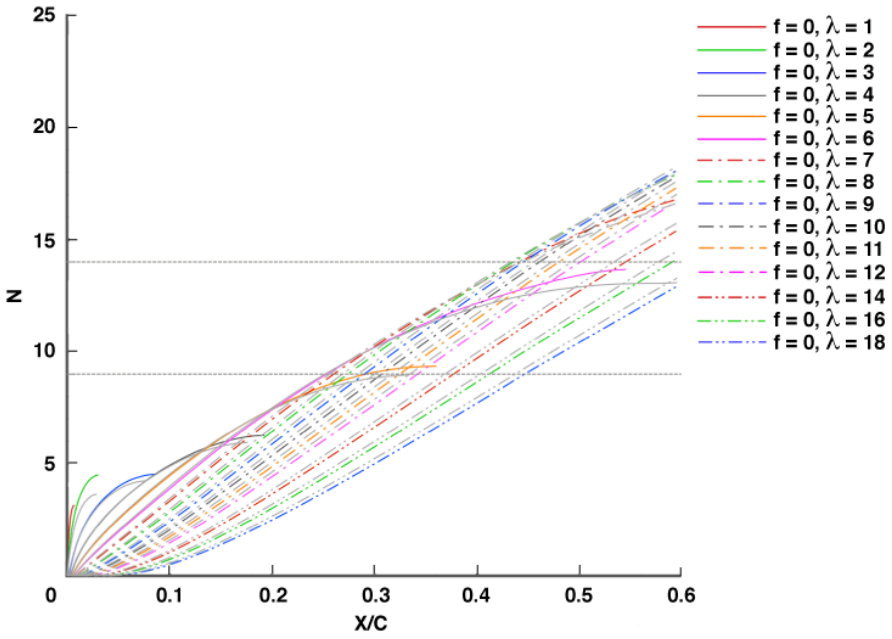

Figure 23. Optimized glove section (BL234) LST N-factors in DRE regime: M = 0.75; Re_c = 22 million (c = 4.4 m, H = 43,610 ft). Dashed horizontal lines show expected transition N-factors for polished (N_{tr} = 14) and operational (N_{tr} = 9) LE roughness. Spanwise wavelengths are in mm. Grey lines show LST results for Target C_p.

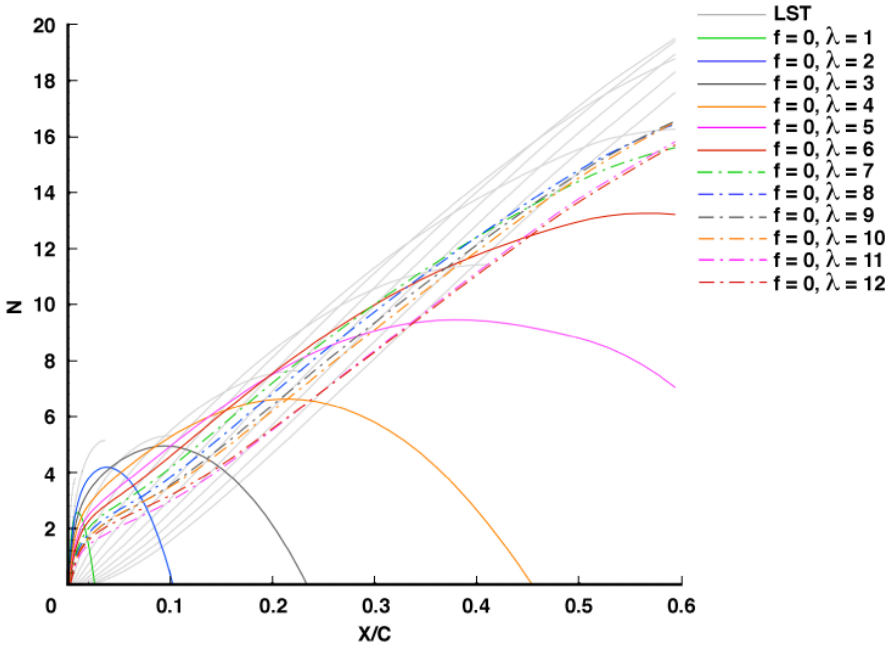

Figure 24. Optimized glove section (BL234) LPSE N-factors in DRE regime: M = 0.75; Re_c = 22 million (c = 4.4 m, H = 43,610 ft). Spanwise wavelengths are in mm. Grey lines show glove LST results for same conditions (Figure 23).

VII. Conclusions

The final glove design that is a result of the 3D optimization process shows stability characteristics that make the glove a good candidate to demonstrate the application of discrete roughness elements at transport relevant chord Reynolds numbers. Additionally, the effectiveness of the optimization can be conclusively verified using parabolized stability equation computations (both linear and nonlinear) on boundary-layer profiles from a fully viscous 3D Navier-Stokes solution. The present boundary-layer solutions used in the stability analyses assume an infinite swept wing. Furthermore, LST does not account for curvature, nonlinear, and non-parallel effects. Initial LPSE calculations agree with the LST

results, but additional computations are warranted for final assessment of the design. These efforts are currently in progress.

The entire optimization process evolved with the addition of new and modified constraints, objectives, and geometry perturbation methods. Additions and modifications to the geometry perturbation significantly affected the smoothness, shape, and increased the possible final shapes from the optimization. Including some constraints in the process restricts the optimization so only viable candidates are produced. The problem, however, should not be over constrained, which could unnecessarily limit the optimizer and lead to increased solution times. Even though the design objectives may be clear in the user's mind, the objective function evolves throughout the design process to best achieve the desired results. The function is sensitive to format and weighting, and can be modified to fit the user's needs exactly. If the constraints, objective, or geometry perturbation functions are not formulated well, the optimizer will undoubtedly find 'holes' and most likely produce a non-ideal solution. This solution could violate some constraints that needed to be imposed, or could very poorly satisfy the design objectives.

The final optimization parameters that were found to yield the best optimized glove shape are as follows. The geometry perturbation function used 24^{th} order curves chordwise, and 7^{th} order curves spanwise. Seven nodes on each span slice are used as constraints that are spread out over each airfoil section to ensure the necessary clearances are maintained everywhere. The objective function matched the C_p distributions of the glove at 5 span stations to one target C_p distribution. The function at each of the five span stations was a weighted sum of C_p value and slope matching with a weighted ratio of 2:1 respectively. The optimized shape improved every time the optimizer was initialized using the previously optimized glove shape.

VIII. Discussion & Future Work

Since the optimization process considered different target C_p distributions during the development phase, some insights were gained into the effect that different pressure distributions have on the ability of the optimization routine to match the target. However, due to time constraints, no formal sensitivity study was conducted that would demonstrate the robustness of the method. It is worth noting, although the final target C_p distribution resulted in a glove with LST results that compare favorably with the target, the spanwise uniformity is not as good as it was with some intermediate C_p distributions that had lower pressures on the suction side. It is worth considering, therefore, whether or not a better balance could be achieved with another target C_p that is closer to what the optimizer actually achieved. It would be interesting to use the final center-span C_p as a new target C_p, to see if the optimizer could improve the spanwise uniformity with a target C_p that is bounded by the optimized pressure distributions on the glove rather than uniformly higher than all of the optimized distributions.

Although this design considered a single-point optimization, the process could be extended to multi-point optimization. Such an optimization could be important in an experiment of this type having multiple objectives at different ranges: e.g. NLF in a lower Re_c range and DRE laminar flow control in a higher range. A related consideration is Mach number: the experiment may consider laminar flow at lower Mach numbers, depending on the effects that the supersonic regions are observed to have on boundary-layer stability. In flights at lower Mach numbers where the entire flow over the glove is subsonic, it is possible that the pressure distribution at these lower Mach numbers may not have the desired characteristics. If this is the case, multi-point optimization would be desirable in order to avoid unnecessarily limiting the flight conditions that could be explored without having to construct additional test articles for different regimes.

Multi-point optimization may also be worth considering when including the effects of wing deformation in flight, which is important since a wing glove is mounted directly on the host aircraft wing and will deform in flight. Some preliminary studies suggest that the effects of wing deformation are accountable, but further study is necessary to conclusively understand the effects that wing deformation will have on the experiment.

The design process should not be limited, however, to the design at hand. As discussed in this paper, an optimization process required experience to design and execute a well-formulated optimization problem. The experience and knowledge gained from this optimization has added a new capability that can be harvested for use in future projects.

Acknowledgments

The authors would like to thank David Bogue and Garvin Forrester at Calmar Research Corporation for their support with TRANAIR. David Bogue helped develop and implement the CST routine and objective functions into TRANAIR. He provided good examples for the implementation and assisted in the development of successful routines used in this paper. Garvin Forrester provided generous assistance to Texas A&M University in the process of procuring TRANAIR.

The authors would also like to thank Prof. William Saric (DRELFGE Co-Principal Investigator) at Texas A&M for his guiding insights into the stability results and the desired characteristics of the optimized design and Matthew Roberts, also at Texas A&M, for his assistance with model construction and drawings.

Portions of this work at Texas A&M were supported under ViGYAN sub recipient grant number C10-00350 and Alliant Techsystems (ATK) sub recipient grant SP00029509 administered through NASA Langley Research Center. The present work is a partnership with NASA Langley Research Center and NASA Dryden Flight Research Center. Technical interactions with the NASA Centers are gratefully acknowledged.

References

[1]Saric, W. S., Carpenter, A. L., and Reed, H. L., "Passive Control of Transition in Three-Dimensional Boundary Layers, with Emphasis on Discrete Roughness Elements," *Philosophical Transactions of The Royal Society A*, Vol. 369, No. 1940, April 2011, pp. 1352–64.

[2]Belisle, M. J., Neale, T. P., Reed, H. L., and Saric, W. S., "Design of a Swept-Wing Laminar Flow Control Flight Experiment for Transonic Aircraft," AIAA-2010-4381, 2010.

[3]Belisle, M. J., Roberts, M. W., Tufts, M. W., Tucker, A. A., Williams, T. C., Saric, W. S., and Reed, H. L., "Design of the Subsonic Aircraft Roughness Glove Experiment (SARGE)," AIAA-2011-3524, 2011.

[4]Haney, H. P., and Waggoner, E. G., "Computational Transonic Wing Optimization and Wing Tunnel Test of a Semi-Span Wing Model," AIAA-1978-0102, 1978.

[5]Jou, W. H., Huffman, W. P., Young, D. P., Melvin, R. G, Bieterman, M. B., Hilmes, C. L., and Johnson, F. T., "Practical Considerations In Aerodynamic Design Optimization," AIAA-1995-1730, 1995.

[6]Ronzheimer, A., Natterer, F. J, and Brezillon, J., "Aircraft Wing Optimization Using High Fidelity Closely Coupled CFD and CSM Methods," AIAA 2010-9078, 2010.

[7]Rhodes, R. G., Reed, H. L., Saric, W. S., and Carpenter, A. L., "Roughness Receptivity in Swept-Wing Boundary Layers-Computations," *International Journal of Engineering Systems Modelling and Simulation*, Vol. 2, No. 1, 2010, pp. 139–48.

[8]*TRANAIR User's Manual*, The Boeing Company, 2009.

[9]Chang, C., "The Langley Stability and Transition Analysis Code (LASTRAC): LST, Linear & Nonlinear PSE for 2-D, Axisymmetric, and Infinite Swept Wing Boundary Layers," AIAA-2003-0974, 2003.

[10]Pruett, C. D., "A Spectrally Accurate Boundary-Layer Code for Infinite Swept Wings," NASA CR-195014, 1994.

[11]Malik, M., "Boundary-Layer Transition Prediction Toolkit," AIAA-1997-1904, 1997.

[12]Bogue, D., and Crist, N., "CST Transonic Optimization Using Tranair++," AIAA-2008-321,2008.

[13]Kulfan, B. M., and Bussoletti, J. E., "Fundamental Parametric Geometric Representations for Aircraft Component Shapes," AIAA-2006-6948, 2006.

[14]Kulfan, B. M., "A Universal Parametric Geometry Representation Method - "CST"," AIAA-2007-62, 2007.

[15]Lane, K. A., "Novel Inverse Airfoil Design Utilizing Parametric Equations," Thesis, California Polytechnic State University, San Luis Obispo, California, 2010.

[16]Mousavi, A., Castonguay, P., and Nadarajah, S. K., "Survey of Shape Parameterization Techniques And Its Effect On Three-Dimensional Aerodynamic Shape Optimization," AIAA-2007-3837, 2007.

[17]Saric, W. S., Reed, H. L., and White, E. B. "Stability and Transition of Three-Dimensional Boundary Layers," *Annual Review Fluid Mechanics*, Vol. 35, 2003, pp. 413–440.

[18]Malik, M., Liao, W., Lee-Rausch, E., Li, F., Choudhari, M., and Chang, C., "Computational Analysis of the G-III Laminar Flow Glove," AIAA-2011-3525, 2011.